

Intracranial Lesions with High Signal Intensity on T1-weighted MR Images: Differential Diagnosis¹

Daniel T. Ginat, MD, MS • Steven P. Meyers, MD, PhD

CME FEATURE

See www.rsna.org/education/lrg_cme.html

LEARNING OBJECTIVES FOR TEST 4

After completing this journal-based CME activity, participants will be able to:

- List the substances that may produce high signal intensity at T1-weighted MR imaging.
- Explain the physical basis for the T1-hyperintense signal produced by each substance.
- Formulate a differential diagnosis for intracranial lesions with high signal intensity at T1-weighted imaging.

TEACHING POINTS

See last page

Various substances, including methemoglobin, melanin, lipid, protein, calcium, iron, copper, and manganese, are responsible for the intrinsically high signal intensity observed in intracranial lesions at T1-weighted magnetic resonance (MR) imaging. Many of these substances have physical properties that lead to other specific imaging features as well. For example, lipid-containing lesions frequently produce chemical shift artifact, and some melanin-containing lesions exhibit a combination of high signal intensity on T1-weighted images and low signal intensity on T2-weighted images. The location and extent of a region of abnormal signal hyperintensity may be helpful for identifying rare diseases such as an ectopic posterior pituitary gland near the floor of the third ventricle, bilateral involvement of the dentate and lentiform nuclei in Cockayne syndrome, and involvement of the anterior temporal lobe and cerebellum in neurocutaneous melanosis. In cases in which diagnostically specific T1-weighted imaging features are lacking, findings obtained with other MR pulse sequences and other modalities can help narrow the differential diagnosis: An elevated glutamine or glutamate level at MR spectroscopy is suggestive of hepatic encephalopathy; a popcorn ball-like appearance at T2-weighted imaging, of cavernous malformations; and hyperattenuation at computed tomography, of mineral deposition disease. In many cases, a comparison of imaging features with clinical measures enables a specific diagnosis.

©RSNA, 2012 • radiographics.rsna.org

Table 1
Classification of T1-Hyperintense Intracranial Lesions according to Lesion Content

Content	Lesion
Methemoglobin	Hemorrhagic infarct, intraparenchymal hematoma (eg, in amyloid angiopathy), diffuse axonal injury, subarachnoid hemorrhage, epidural hematoma, subdural hematoma, intraventricular hemorrhage, arterial and venous thrombi, vascular malformations (eg, cavernous malformation), hemorrhagic neoplasm
Melanin	Metastatic melanoma, primary diffuse meningeal melanomatosis, melanocytoma, neurocutaneous melanosis
Lipid	Lipoma, osteolipoma, teratoma, dermoid cyst, lipomatous neoplasm (meningioma, astrocytoma, medulloblastoma, neurocytoma, ependymoma), hypothalamic hamartoma, metaplastic ossification of the dura
Protein	Colloid cyst, Rathke cleft cyst, ectopic posterior pituitary gland, intracranial extension of mucocele, duplicated pituitary gland
Minerals	Cockayne syndrome, Fahr disease (hypoparathyroidism, pseudohypoparathyroidism, pseudopseudohypoparathyroidism; tumor calcification), neurodegeneration with brain iron accumulation, Fabry disease, hepatic encephalopathy, Wilson disease, hyperalimentation, hypermagnesemia
Other	HIV infection, type 1 neurofibromatosis, cholesterol granuloma, craniopharyngioma, cortical laminar necrosis, hypoxic ischemic encephalopathy, chronic multiple sclerosis, chordoma, nonketotic hyperglycemia, abscess

Note.—HIV = human immunodeficiency virus.

Introduction

T1 (spin-lattice) relaxation is the process of longitudinal magnetization recovery after application of a radiofrequency pulse, or excitation, to invert the magnetization vector (1,2). This process occurs as energy from the spinning nuclei is dissipated into the surrounding areas. T1 is the time required for spins to recover approximately 63% of their preexcitation magnetization. Substances that have intrinsically shorter T1 relaxation times demonstrate higher signal intensity at T1-weighted imaging. The specific effect of T1 weighting on the imaging appearance of a substance depends on the repetition time, echo time, proton density, and magnetic field strength (1,2). These parameters have interactive effects. Of note, gains in signal-to-noise ratio with increasing field strengths can be undermined by the resultant prolongation of T1 relaxation times (3,4).

Only a few naturally occurring substances are known to reduce T1 relaxation times, and the extent of that reduction depends on their occurrence in substantial concentrations. These substances include methemoglobin, melanin, lipid, protein, and minerals. However, in some cases, the high signal intensity seen in lesions has

not been definitively linked to any of these substances. Nevertheless, familiarity with the effect of chemical composition on T1 signal intensity facilitates the differential diagnosis of lesions that have a high-signal-intensity appearance on T1-weighted images (Table 1). These lesions can be further categorized on the basis of their location (Table 2). In addition, consideration of other imaging features and clinical variables can help narrow the differential diagnosis and in some cases enable a specific diagnosis.

The article reviews the fundamental physical properties of substances that produce T1 signal hyperintensity, providing a solid conceptual basis for formulating a comprehensive differential diagnosis of T1-hyperintense intracranial lesions. Common and uncommon entities that appear bright on T1-weighted magnetic resonance (MR) images are described in detail.

Methemoglobin-containing Lesions

Physical Properties

The MR imaging appearance of intracranial hemorrhages and other lesions that contain blood products largely depends on the age of the blood. Both intracellular methemoglobin (early subacute phase hemorrhage, 3–7 days after onset)

Table 2
Classification of T1-Hyperintense Intracranial Lesions according to Lesion Location

Location	Lesion
Deep gray matter nuclei	Cockayne syndrome: lentiform and dentate nuclei Pantothenate kinase-associated neurodegeneration: bilateral in globus pallidus and substantia nigra Hypertensive hemorrhage: unilateral or bilateral in putamen, external capsule, and thalamus Hepatic encephalopathy: bilateral in globus pallidus and substantia nigra Hyperalimantation: same as hepatic encephalopathy Hypoxic ischemic injury: lateral aspect of thalamus, posterior aspect of putamen and hippocampus Fabry disease: pulvinar nuclei only Fahr disease: bilateral and symmetric in basal ganglia, thalamus, dentate nucleus, and centrum semiovale Hypoparathyroidism, pseudohypoparathyroidism, and pseudopseudohypoparathyroidism: similar to Fahr disease Lead, cyanide, and methanol poisoning: bilateral in putamen Type 2 neurofibromatosis: bilateral in globus pallidus and internal capsule Wilson disease: bilateral in basal ganglia and thalamus Nonketotic hyperglycemia: bilateral in caudate nucleus and globus pallidus HIV infection: caudate nucleus and putamen Neurodegenerative Langerhans cell histiocytosis: putamen
Cerebral hemisphere	Amyloid angiopathy, hemorrhagic metastasis or primary tumor, lipomatous ependymoma, vascular malformation, hemorrhagic contusion, hemorrhagic infarct, cortical laminar necrosis
Midline structures	Dermoid cyst, teratoma, lipoma, osteolipoma, hypothalamic hamartoma, pituitary microhemorrhage and apoplexy, deep cerebral vein thrombosis
Suprasellar and sellar compartment	Hypothalamic hamartoma, dermoid cyst, teratoma, craniopharyngioma, Rathke cleft cyst, ectopic posterior pituitary lobe, lipoma, osteolipoma, thrombosed aneurysm of circle of Willis, Langerhans cell histiocytosis, pituitary microhemorrhage and apoplexy
Ventricles	Intraventricular hemorrhage, colloid cyst (in third ventricle), ruptured dermoid cyst
Dura mater	Lipomatous meningioma, hemorrhagic metastasis, melanoma, venous sinus thrombosis

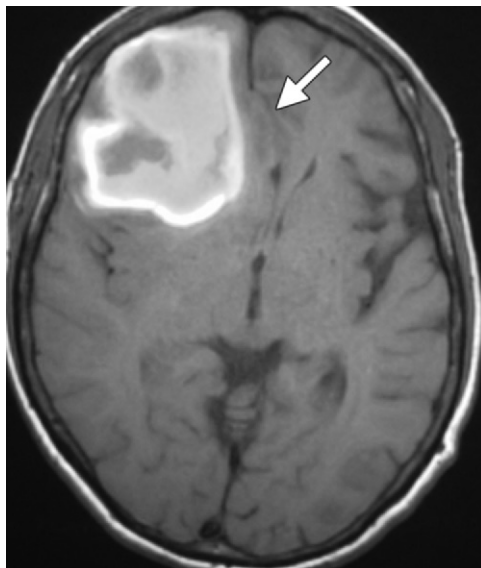
Note.—HIV = human immunodeficiency virus.

and extracellular methemoglobin (late subacute phase hemorrhage, from 8 days to 1 month after onset) produce T1 shortening effects on adjacent hydrogen nuclei in water and other molecules and therefore have intrinsically high signal intensity on T1-weighted images. The short T1 of methemoglobin is attributed to paramagnetic dipole-dipole interactions (5). Intracellular methemoglobin has a shorter T2 than extracellular methemoglobin, so a comparison of T1-weighted images with T2-weighted images can help distinguish between the two.

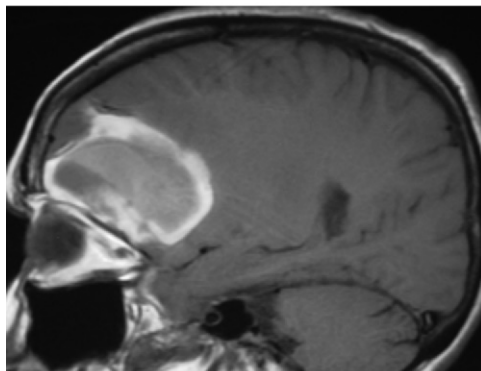
Amyloid Angiopathy

Cerebral amyloid angiopathy is a disorder of β -amyloid deposition in cortical, subcortical, and leptomeningeal vessels (6). Although this

condition is responsible for only about 2% of all intracranial hemorrhages, it is relatively common among the elderly (6). According to the Boston criteria, a definitive diagnosis of amyloid angiopathy is based on a positive finding at autopsy (7). However, MR imaging may provide evidence suggestive of the diagnosis. For example, petechial microhemorrhages or macrohemorrhages with irregular borders in a lobar distribution in cortical and subcortical regions are characteristic findings of amyloid angiopathy (Fig 1). Intraparenchymal hemorrhages at various stages of evolution, as well as subarachnoid, subdural, and intraventricular hemorrhages, may be seen at imaging.



a.

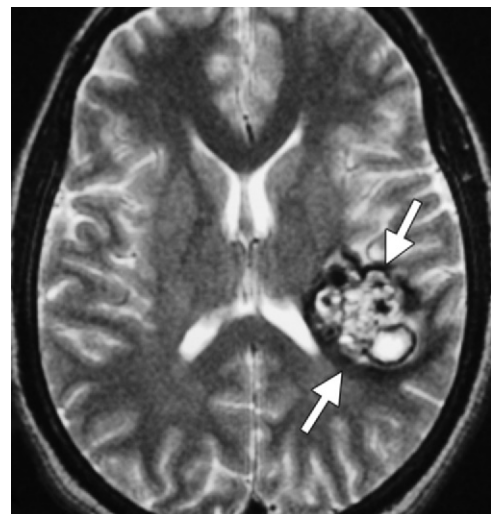


b.

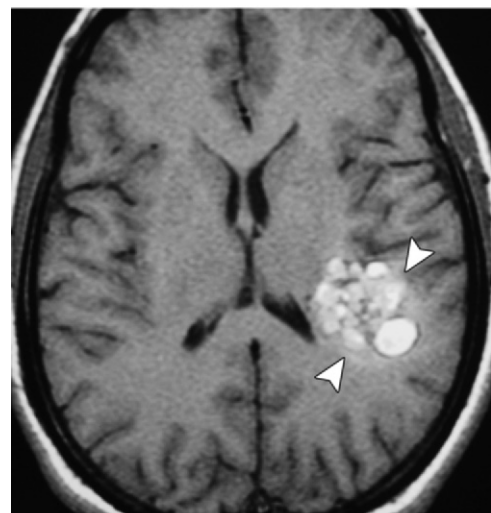
Figure 1. Amyloid angiopathy in a 71-year-old woman. Axial (**a**) and sagittal (**b**) T1-weighted MR images show a large right frontal hemorrhage that involves both the cortex and white matter, with resultant subfalcine herniation (arrow in **a**). The hemorrhage is predominantly subacute, as evidenced by high signal intensity, especially at the periphery of the lesion.

Cavernous Malformations

Cavernous malformations (eg, cavernous angiomas) are congenital or acquired vascular anomalies that occur in approximately 0.5% of the general population (8). Patients may present with seizures and neurologic deficits. Classic features seen at T2-weighted and T2*-weighted MR imaging include a lesion with a popcorn ball-like appearance and a low-signal-intensity rim due



a.



b.

Figure 2. Intracranial cavernous malformation in a 32-year-old man. (**a**) Axial T2-weighted MR image shows a large left parietal mass that resembles a popcorn ball, with a hypointense hemosiderin rim (arrows) and loculated hyperintense compartments. (**b**) Axial T1-weighted MR image at the same level shows multiple high-signal-intensity compartments in the lesion, findings suggestive of subacute hemorrhage. A faint halo of high signal intensity also is visible around the lesion (arrowheads).

to hemosiderin deposition (Fig 2a). **Subacute hemorrhage and degraded blood products within the lesion produce a halo of signal hyperintensity around the lesion on T1-weighted images, a useful finding for differentiating cavernous malformations from hemorrhagic tumors and other intracranial hemorrhages (9) (Fig 2b).** In one study, associated developmental venous anomalies were found in 44% of patients with sporadic cavernous

Teaching
Point

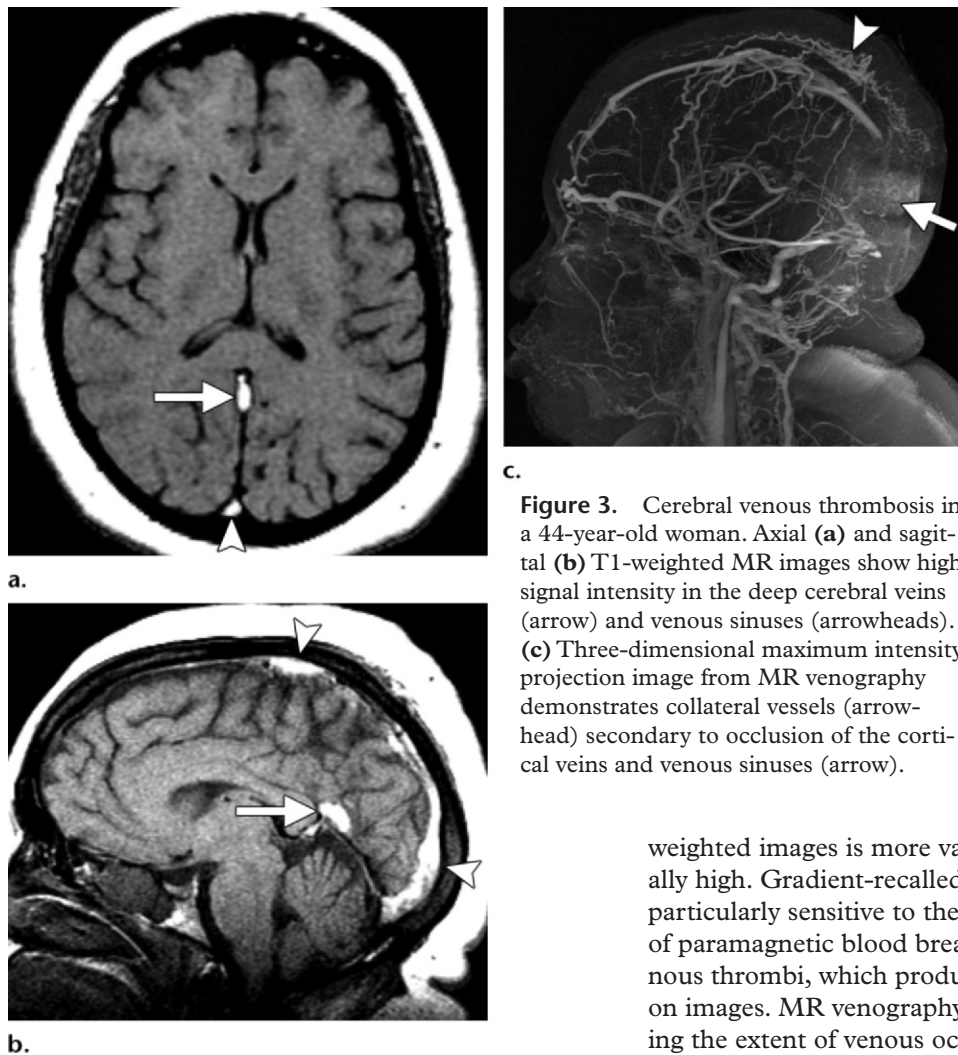


Figure 3. Cerebral venous thrombosis in a 44-year-old woman. Axial (**a**) and sagittal (**b**) T1-weighted MR images show high signal intensity in the deep cerebral veins (arrow) and venous sinuses (arrowheads). (**c**) Three-dimensional maximum intensity projection image from MR venography demonstrates collateral vessels (arrowhead) secondary to occlusion of the cortical veins and venous sinuses (arrow).

angiomas but in few patients with familial cavernous angiomas, a finding likely indicative of a difference in pathogenesis between the two lesion groups (10).

Cerebral Venous Thrombosis

Cerebral venous sinus thrombosis is an unusual condition that most commonly manifests with a headache (11). A characteristic finding at unenhanced computed tomography (CT) is the presence of a hyperattenuating clot, although this feature is apparent in only about 20% of cases. Similarly, the “empty delta” sign, a filling defect at contrast-enhanced CT or CT venography, is present in less than 30% of cases (12). The appearance of venous thrombosis at MR imaging varies, depending mainly on the age of the thrombus at presentation. A subacute thrombus often has high signal intensity on T1-weighted images (Fig 3); the signal intensity on T2-

weighted images is more variable but is also usually high. Gradient-recalled echo sequences are particularly sensitive to the susceptibility effects of paramagnetic blood breakdown products in venous thrombi, which produce blooming artifacts on images. MR venography is effective for depicting the extent of venous occlusion and collateral vessel formation.

Melanin-containing Lesions

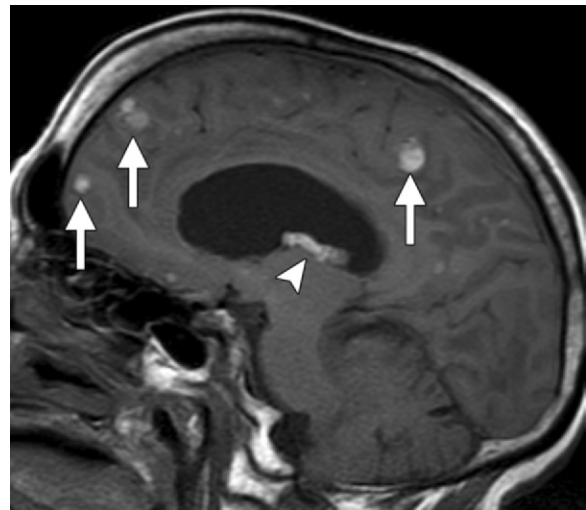
Physical Properties

Melanin-containing lesions demonstrate high signal intensity on T1-weighted images because of the paramagnetic effects of stable free radicals, such as semiquinones, and metal scavenging effects, in which melanin binds to chelated metal ions, forming metallomelanin (13). Furthermore, the signal intensity of metallomelanin on T1-weighted images was found to increase with an increasing iron concentration (14).

Metastatic Melanoma

Intracranial metastases occur in nearly 40% of patients with malignant melanoma (15). In comparison with the signal in normal tissue, the signal in melanotic melanoma is characteristically

Figure 4. Metastatic intracranial melanoma in a 37-year-old woman. Sagittal T1-weighted MR image shows several round high-signal-intensity lesions scattered throughout the cerebral hemispheres, at the junctions of gray and white matter (arrows) and in the choroid plexus (arrowhead).



hyperintense on T1-weighted images and hypointense on T2-weighted images (Fig 4). High signal intensity also can result from hemorrhage within these lesions. Amelanotic metastatic melanoma tends to exhibit signal that is either isointense or hypointense to that in normal tissue on T1-weighted images (16).

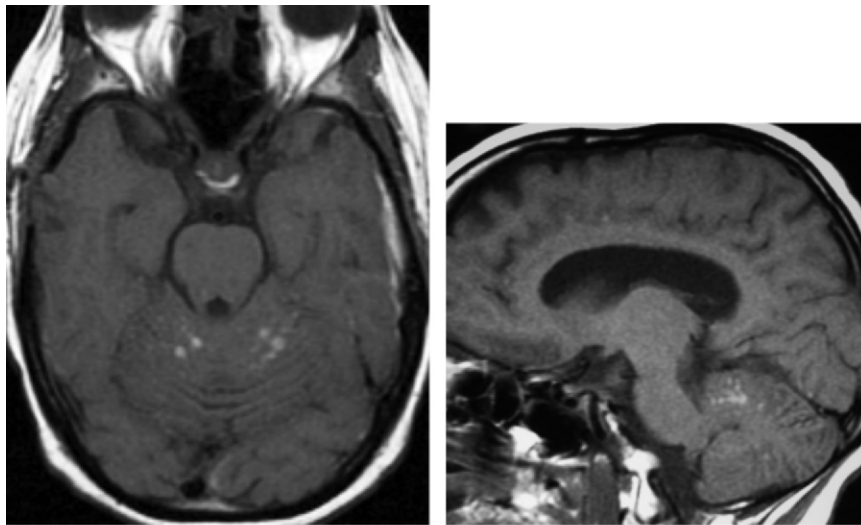
Primary Diffuse Meningeal Melanomatosis

Primary diffuse meningeal melanomatosis is a particularly aggressive form of primary intracranial melanoma. This condition is extremely rare, with an estimated incidence of only five cases per 100 million in the general population, and it occurs more commonly in adults than in children (17,18). Manifestations include seizures, intracranial hypertension, and cranial nerve deficits (18). Although the leptomeninges are the primary site of involvement, the disease process may extend to the dura. The meninges of the spine are also commonly involved and should be examined at MR imaging. The lesions in primary diffuse meningeal melanomatosis display intermediate or high signal intensity on T1-weighted MR images (Fig 5) (17). However, the full extent of disease is best appreciated at contrast-enhanced T1-weighted imaging, when the lesions may demon-

strate avid enhancement. The widespread involvement seen in diffuse meningeal melanomatosis differs greatly from the typically localized manifestation of metastatic melanoma, but a careful search nevertheless must be made for an occult extracranial primary melanoma (18,19). Other differential considerations include hemorrhage, sarcoidosis, infectious meningitis, and meningeal carcinomatosis.

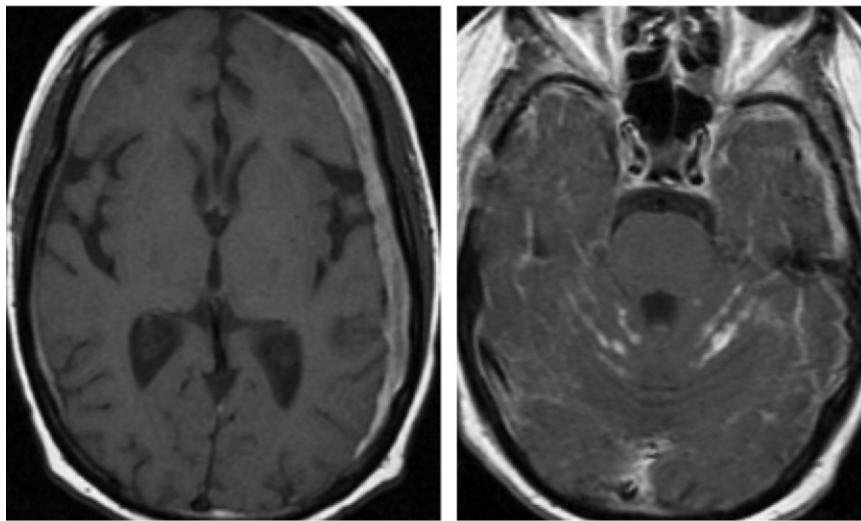
Neurocutaneous Melanosis

Neurocutaneous melanosis is an uncommon congenital condition characterized by multiple giant or hairy pigmented nevi and melanin-containing leptomeningeal lesions without evidence of extracranial melanoma (18,20). Patients may present with hydrocephalus, seizures, or intracranial hemorrhage. Melanoma arises from the leptomeningeal lesions in 40%–60% of cases of neurocutaneous melanosis (20). The intracranial lesions have a predilection for the anterior temporal lobes (Fig 6) and cerebellum. In comparison with normal tissue, the lesions in neurocutaneous melanosis typically appear hyperintense on T1-weighted images and hypointense on T2-weighted images because of the characteristic effects of melanin. The lesions are difficult to discern at CT (18). Findings of lesion enlargement, surrounding edema, mass effect, nodular enhancement, and central necrosis are suggestive of malignant degeneration (18).



a.

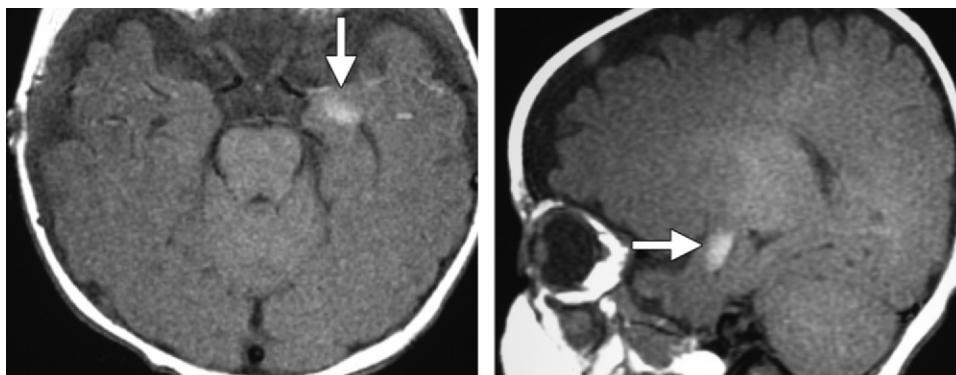
b.



c.

d.

Figure 5. Primary diffuse meningeal melanomatosis in a 27-year-old woman. (a, b) Axial (a) and sagittal (b) T1-weighted MR images demonstrate several high-signal-intensity nodular leptomeningeal foci in the cerebellum. (c) Axial T1-weighted MR image at another level shows diffuse high signal intensity within the thickened dura bilaterally. (d) Axial contrast-enhanced T1-weighted MR image shows more extensive leptomeningeal involvement in and beyond the cerebellum.



a.

b.

Figure 6. Neurocutaneous melanosis in a 1-year-old boy. Axial (a) and sagittal (b) T1-weighted MR images show a focus of high signal intensity (arrow) in the left amygdala. There is no appreciable mass effect.

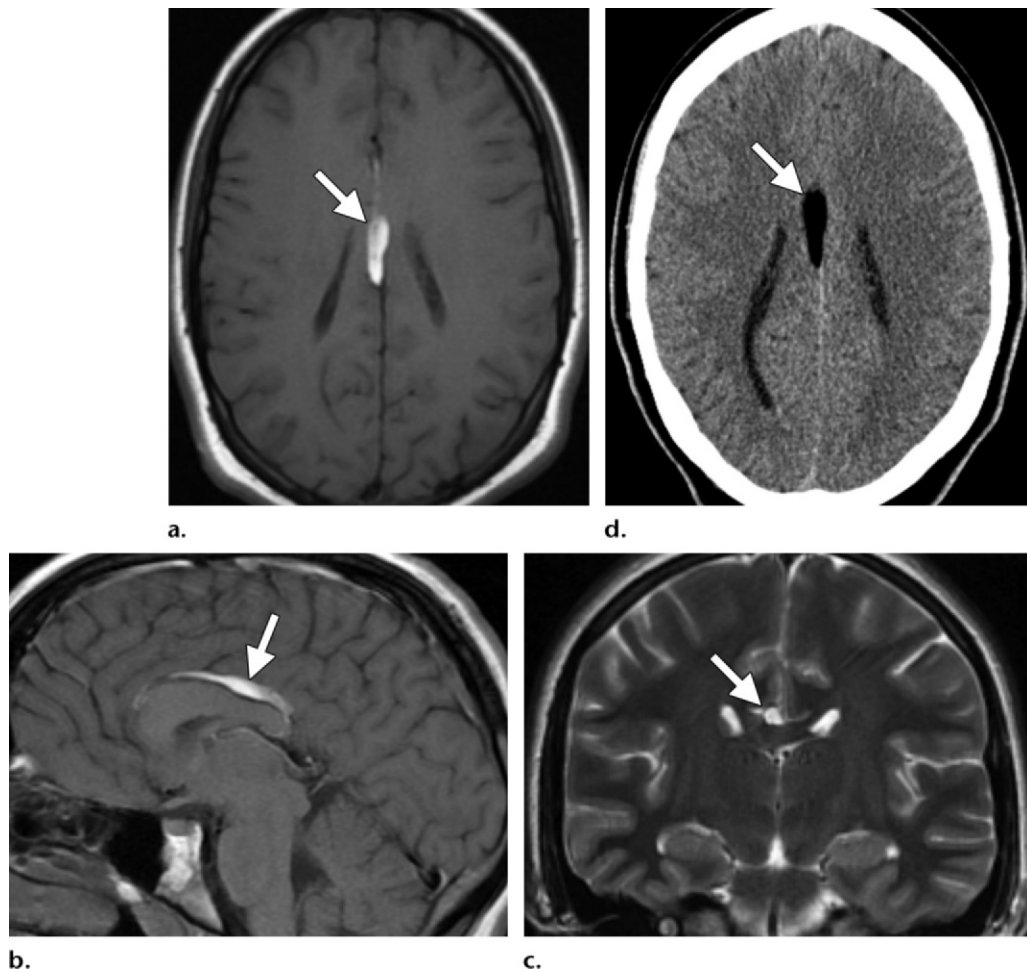


Figure 7. Curvilinear pericallosal lipoma and dysgenesis of the corpus callosum in a 16-year-old girl. **(a, b)** Axial **(a)** and sagittal **(b)** T1-weighted MR images show a linear hyperintense mass along the dorsal aspect of the corpus callosum (arrow). The splenium of the corpus callosum is absent. **(c)** Coronal T2-weighted MR image shows the same high-signal-intensity lesion (arrow) with a chemical shift artifact along its edge in the frequency-encoding direction. **(d)** Axial CT image reveals the homogeneous low attenuation of fat within the lesion (arrow).

Lipid-containing Lesions

Physical Properties

The short T1 relaxation time of hydrogen nuclei within lipid molecules produces high signal intensity on T1-weighted MR images (21). Frequency-selective fat suppression and short inversion time inversion-recovery sequences are routinely used at MR imaging to eliminate this high signal intensity. The difference in the precession frequencies of protons in lipid and protons in water also results in chemical shift artifact at fat-water interfaces, which is a useful property in diagnostic MR imaging. At 1.5 T, this shift results in a 224-Hz separation between the resonance frequen-

cies of fat and water protons (22). The resultant artifact appears as a dark or bright band aligned along the interface, in the direction of frequency encoding (22).

Intracranial Lipomas

Intracranial lipomas are rare congenital malformations that arise from abnormal differentiation of the persistent primitive meninx (23,24). Intracranial lipomas most commonly occur in the pericallosal region (25). Two morphologic types of pericallosal lipomas have been described: tubulonodular and curvilinear (Fig 7). Although benign and often asymptomatic, pericallosal lipomas, particularly those of the more anteriorly located tubulonodular type, are frequently associated with dysgenesis or agenesis of the

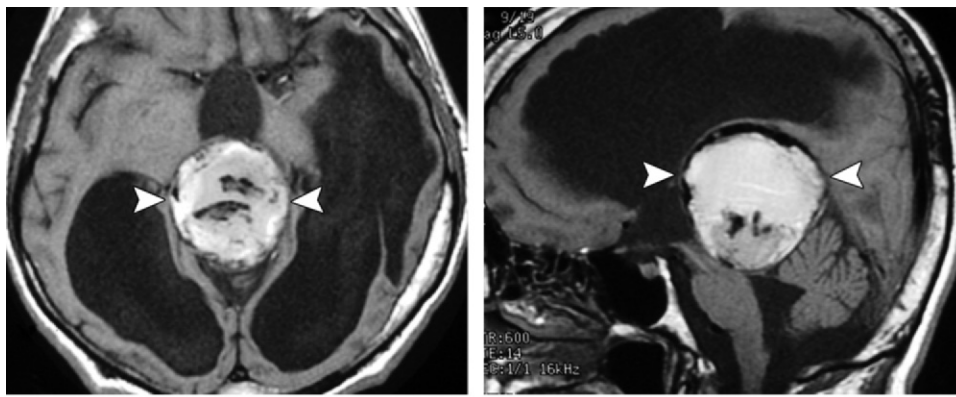


Figure 8. Pineal teratoma in a 2-year-old boy. Axial (**a**) and sagittal (**b**) T1-weighted MR images show a large, heterogeneous pineal gland mass (arrowheads) and severe obstructive hydrocephalus.

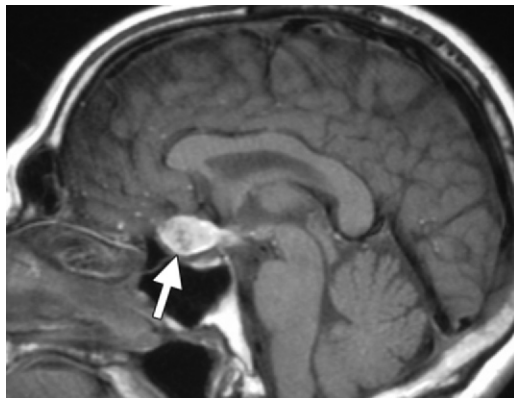


Figure 9. Ruptured dermoid cyst in a 44-year-old woman. Sagittal T1-weighted MR image shows an ovoid, heterogeneously hyperintense midline suprasellar mass (arrow) and numerous punctate high-signal-intensity foci scattered throughout the subarachnoid space.

corpus callosum (24). Intracranial lipomas also have a predilection for the quadrigeminal plate, quadrigeminal cistern, sylvian fissure, and dorsal perimesencephalic region. Of note, lipomas in the sylvian fissure are strongly associated with seizure activity (25). The lesions are readily identifiable at imaging, with fat attenuation at CT and signal intensity characteristics of adipose tissue at MR imaging, including fat-suppressed imaging (25). Vessels and nerves also may be seen to traverse the lesions.

Teratomas

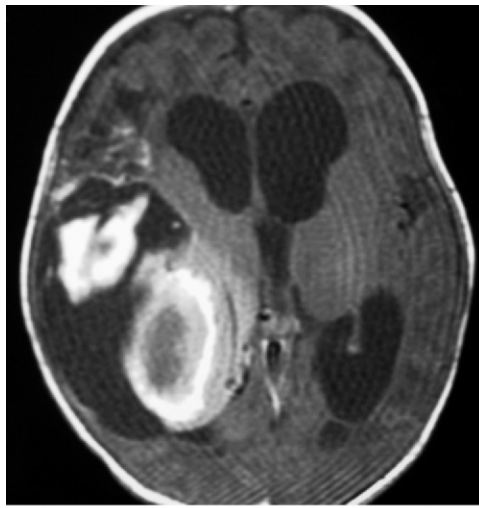
Intracranial teratomas are true neoplasms that usually contain tissue derived from all three germ cell layers, but they also can arise from a single germ cell layer if cellular differentiation

is disturbed (26). Most intracranial teratomas are benign, although mature, immature, and malignant variants exist. Overall, teratomas are the most common congenital intracranial tumor and are usually diagnosed prenatally (27). Intracranial teratomas are most frequently found in the cerebral hemispheres and pineal gland. At MR imaging, they typically manifest as multiloculated cystic lesions that contain calcifications and fat, which are responsible for their high-signal-intensity appearance on T1-weighted images (Fig 8).

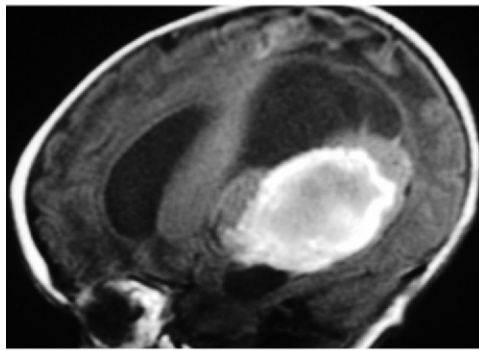
Dermoid Cysts

Dermoid cysts are rare, benign, congenital ectodermal inclusion cysts that account for approximately 0.3% of all intracranial tumors (28,29). Intracranial dermoid cysts most commonly occur at the midline in the sellar and parasellar compartments, fourth ventricle, and vermis (29). The lesions are usually well-defined, non-enhancing masses with fat attenuation at CT. At MR imaging, dermoid cysts typically show high signal intensity on T1-weighted images, variable signal intensity on T2-weighted images, and lack of enhancement on contrast-enhanced images (29). **Dermoid cyst rupture is a rare complication that can cause severe chemical meningitis and sensory or motor hemisyndrome (28,30). This complication manifests at T1-weighted MR imaging as scattered high-signal-intensity foci within the ventricles or subarachnoid spaces (Fig 9).** MR spectroscopy discloses mobile lipid peaks at 0.9 and 1.3 ppm (28).

Teaching
Point

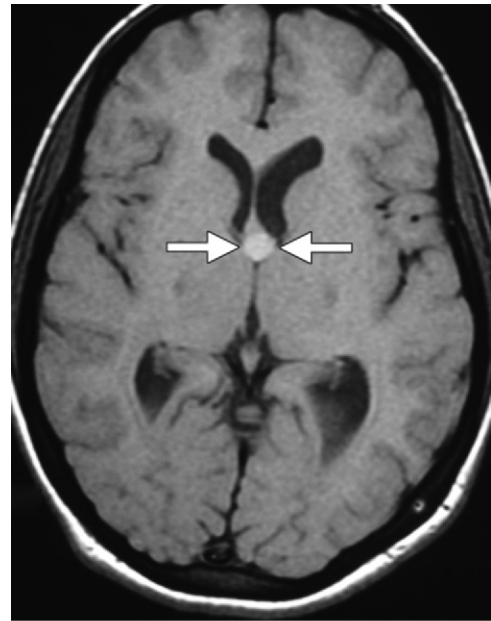


a.

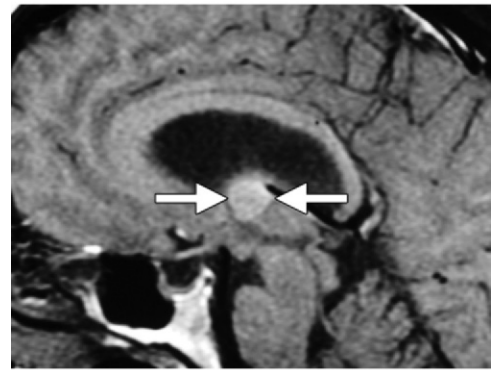


b.

Figure 10. Right supratentorial lipomatous ependymoma in a 3-year-old boy. Axial (**a**) and sagittal (**b**) T1-weighted MR images show a large right supratentorial mass that contains cystic and solid components, with resultant noncommunicating hydrocephalus. A substantial portion of the tumor appears hyperintense; this area represents the solid lipomatous component.



a.



b.

Figure 11. Colloid cyst in a 31-year-old woman. Axial (**a**) and sagittal (**b**) T1-weighted MR images show an ovoid, homogeneously hyperintense lesion at the left foramen of Monro (arrows).

Lipomatous Ependymomas

Ependymoma with lipomatous differentiation is a rare variant of ependymoma in which tumor cells contain lipid droplets (31,32). Many lipomatous ependymomas show hyperintense signal on T1-weighted images (Fig 10). Apart from this characteristic, they display the usual features of other types of ependymomas, including calcification,

hemorrhage, and cystic components. Lipomatous ependymomas tend to occur in the pediatric population and are slow growing (32). However, the prognostic significance of lipomatous differentiation is uncertain.

Protein-containing Lesions

High signal intensity in certain lesions on T1-weighted images can be attributed to their protein content and the hydration layer effect.

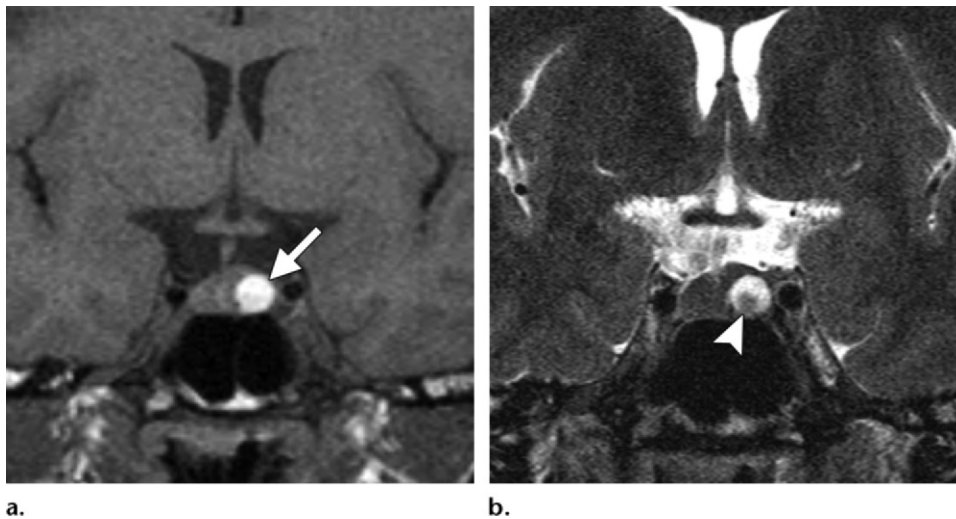


Figure 12. Rathke cleft cyst in a 34-year-old woman with a slightly elevated prolactin level. **(a)** Coronal T1-weighted MR image shows a high-signal-intensity spheroid lesion (arrow) within the sella. **(b)** Coronal T2-weighted MR image shows a low-signal-intensity intracystic nodule (arrowhead) within the spheroid lesion.

Cross-relaxation between the proteins and bound water affects the relaxation rate of free water (33). In addition, macromolecular docking decreases T1 by slowing the mean motional state of the proteins (33). Ultimately, both T1 and T2 relaxation times are dependent on the amount of free water, protein content, and viscosity within these lesions (34).

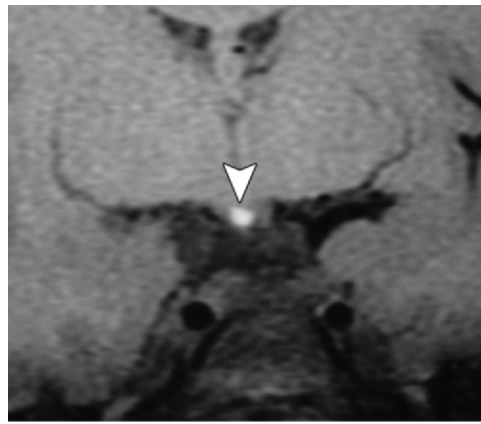
Colloid Cyst

Colloid cysts are uncommon benign intracranial lesions containing a gelatinous material that reacts positively at periodic acid–Schiff staining (35). These lesions characteristically occur at the anterosuperior aspect of the third ventricle and may obstruct the adjacent foramen of Monro. A headache is the most common clinical manifestation in symptomatic patients. Other symptoms may include atonic seizures, nausea, vomiting, diplopia, transient loss of consciousness, and (rarely) sudden death (33). At CT, most of these lesions show hyperattenuation (29). Rimlike enhancement can occur, but calcifications are rare. About two-thirds of colloid cysts show high signal intensity at T1-weighted MR imaging, and most exhibit low signal intensity at T2-weighted imaging (Fig 11) (29,35). Colloid cysts that show low signal intensity at T1-weighted imag-

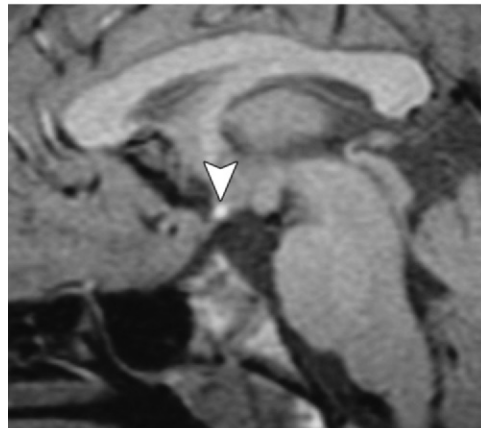
ing and high signal intensity at T2-weighted imaging have a tendency to enlarge rapidly (29).

Rathke Cleft Cyst

Rathke cleft cysts are common benign remnants of the Rathke cleft that may be located in the sellar compartment, the suprasellar compartment, or both (33,36). Although most such cysts are found incidentally, they occasionally cause headaches, visual disturbances, and diabetes insipidus. About half of Rathke cleft cysts show hyperintense signal at T1-weighted imaging (Fig 12). The lesions also frequently appear hyperintense at T2-weighted imaging. Small intracystic nodules with high signal intensity at T1-weighted imaging and low signal intensity at T2-weighted imaging are present in approximately 45% of cases (Fig 12) and are considered a characteristic feature of Rathke cleft cysts (37). Peripheral enhancement is sometimes noted at MR imaging and probably represents underlying metaplasia, inflammation, or deposition of hemosiderin or cholesterol in the cyst wall; however, internal enhancement is never seen (38). A correlation has been found between the presence of peripheral enhancement and an increased risk of recurrence after surgical resection (38).



a.

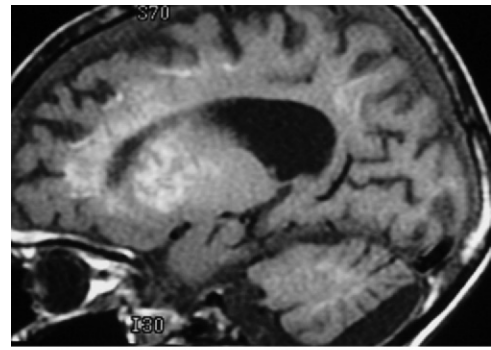


b.

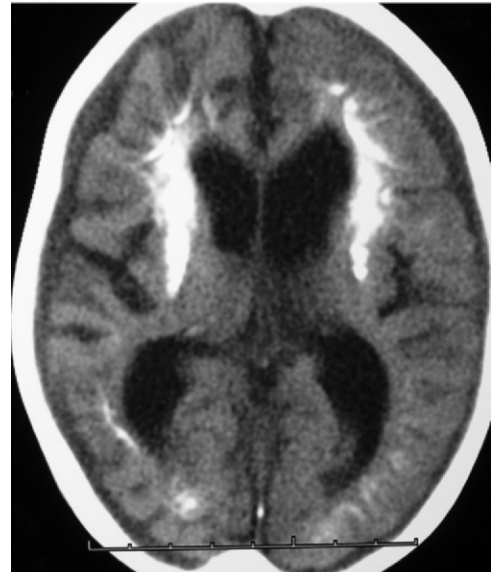
Figure 13. Ectopic posterior pituitary lobe in a 10-year-old girl. Coronal (a) and sagittal (b) T1-weighted MR images show a focus of hyperintense signal (arrowhead) located at the midline, along the anterior tuber cinereum.

Ectopic Posterior Pituitary Gland

Posterior pituitary ectopia is a rare congenital malformation of the hypothalamus that is associated with hypoplasia or absence of the pituitary stalk and resultant dwarfism due to growth hormone deficiency (39). This condition may be associated with septo-optic dysplasia and periventricular heterotopias. The ectopic posterior pituitary lobe is most commonly located along the median eminence in the floor of the third ventricle (Fig 13). An ectopic posterior pituitary gland also might result from traumatic or surgical transection of the pituitary stalk (40,41). Signal hyperintensity in the posterior aspect of the pituitary gland on T1-weighted images is related to the paramagnetic effect of the vasopressin–neurophysin II–copeptin complex (39,42,43).



a.



b.

Figure 14. Cockayne syndrome in a 4-year-old girl. (a) Sagittal T1-weighted MR image shows increased signal intensity in the lentiform nuclei, white matter, and dentate nuclei. Diffuse brain atrophy is visible as well. (b) Axial CT image shows bilateral periventricular dense calcifications.

Mineral-containing Lesions

Calcium and Other Minerals

Calcium is a diamagnetic substance that may appear bright at T1-weighted imaging in specific circumstances. In brain tissue, signal hyperintensity increases in the presence of calcium concentrations of 30% or less by weight (20). At higher concentrations, the intensity of the signal in calcium at T1-weighted imaging diminishes. Furthermore, T1 relaxivity increases with an increase in the surface area of calcifications (20). Other minerals that may have T1 shortening effects include manganese, copper, and iron.

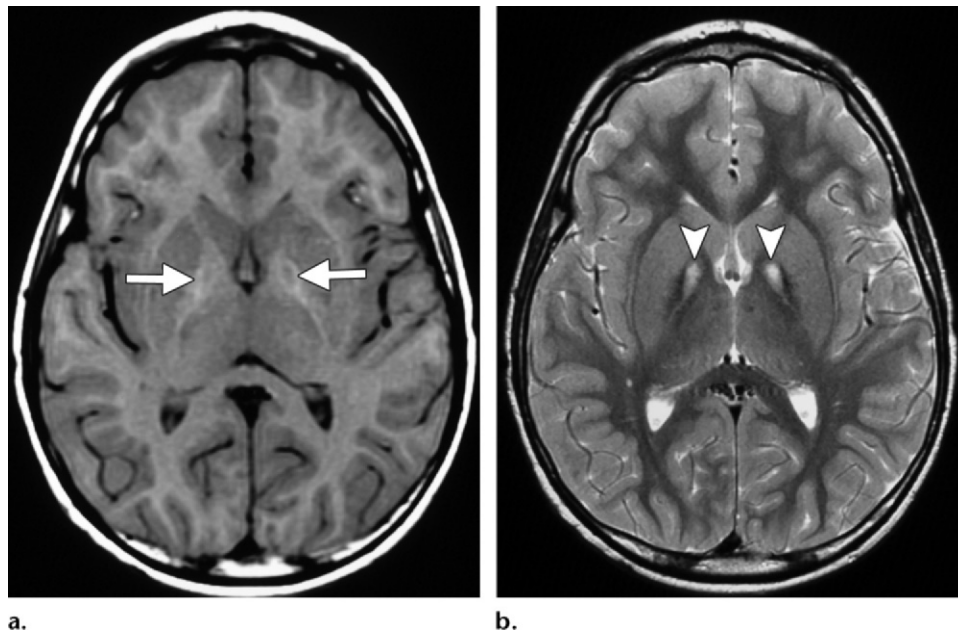


Figure 15. Pantothenate kinase–associated neurodegeneration in a 1-year-old boy. **(a)** Axial T1-weighted MR image shows mild bilateral symmetric hyperintensity of the globus pallidus (arrows). **(b)** Axial T2-weighted MR image shows bilateral areas of high signal intensity in the center of the globus pallidus interna, surrounded by low signal intensity, producing the “eye of the tiger” sign (arrowheads).

Cockayne Syndrome

Cockayne syndrome is an autosomal recessive defect in DNA repair that is characterized clinically by premature aging, encephalopathy, microcephaly, deafness, and photosensitivity (44). Typical imaging findings include cerebral atrophy, white matter hypomyelination, and extensive calcifications within but not limited to the bilateral lentiform and dentate nuclei. These calcifications may exhibit high signal intensity at T1-weighted imaging and low signal intensity at T2-weighted imaging (Fig 14). MR spectra show the presence of lactate and decreased levels of choline and *N*-acetylaspartate in the brains of patients with Cockayne syndrome (44).

Neurodegeneration with Brain Iron Accumulation

Neurodegeneration with iron accumulation in the brain occurs in various disorders, including aceruloplasminemia (caused by ceruloplasmin gene mutation), pantothenate kinase–associated neurodegeneration (due to a mutation in the pantothenate kinase 2 [*PKAN2*] gene), and phospholipase A2 (*PLA2G6*) gene mutation (45). *PKAN2* mutations, which are responsible for most cases of neurodegeneration with brain iron accumulation, result in the accumulation

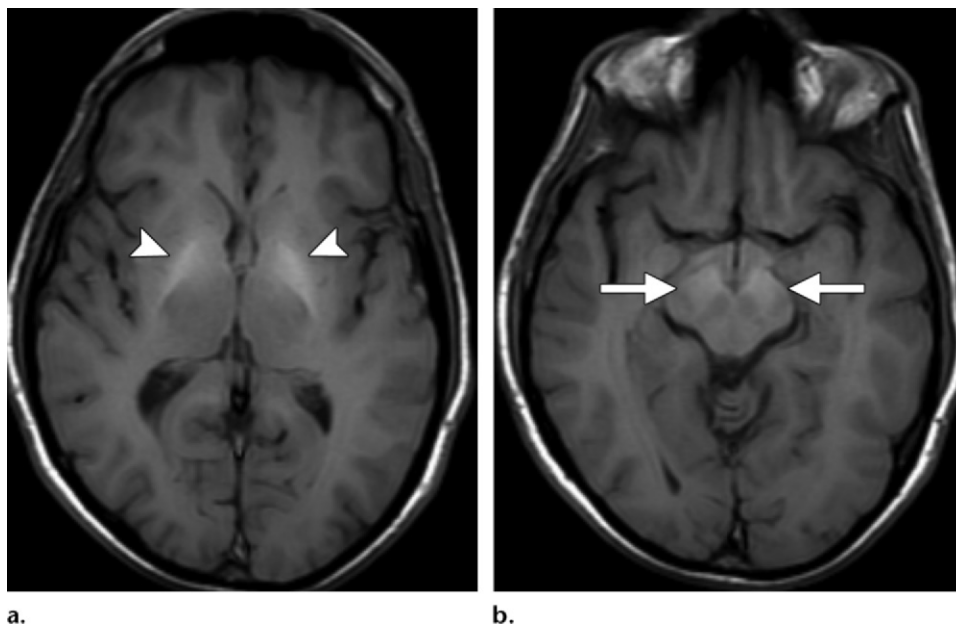
of iron within the globus pallidus and substantia nigra (46,47). This condition manifests clinically as progressive extrapyramidal and pyramidal dysfunction. At T1-weighted MR imaging, the bilateral globus pallidus may sometimes appear hyperintense (Fig 15a). However, at T2-weighted MR imaging, bilateral symmetric foci of signal hyperintensity in the globus pallidus are surrounded by a low-signal-intensity border, producing a characteristic “eye-of-the-tiger” appearance (Fig 15b) (46,47).

Hepatic Encephalopathy

Hepatic encephalopathy may lead to mental status changes and motor dysfunction in patients with underlying liver disease (48). **At MR imaging, hepatic encephalopathy characteristically manifests as bilateral regions of signal hyperintensity in the lentiform nucleus and substantia nigra on T1-weighted images (Fig 16).** These regions of abnormally high signal intensity at T1-weighted imaging are related to the accumulation of manganese in patients with hepatic encephalopathy and may be encountered also in welders and recipients of hyperalimentation therapy. Other findings related to liver disease with or

Teaching
Point

Figure 16. Hepatic encephalopathy in a 60-year-old man. Axial T1-weighted MR images at the level of the basal ganglia (arrowheads in **a**) and substantia nigra (arrows in **b**) show bilateral symmetric regions of hyperintensity in these structures.



without hepatic encephalopathy include diffuse hemispheric signal hyperintensity in white matter along the corticospinal tract on T2-weighted images, focal areas of signal hyperintensity in subcortical white matter on T2-weighted images, and elevated glutamine and glutamate levels at MR spectroscopy that are probably related to ammonia toxicity (48). The brain abnormalities seen at MR imaging and MR spectroscopy in patients with hepatic encephalopathy are potentially reversible with liver transplantation (49,50).

Wilson Disease

Wilson disease is a rare autosomal recessive condition caused by mutations in the *ATP7B* gene with resultant abnormal copper metabolism and accumulation (51). Patients may present with dysarthria, dystonia, tremor, choreoathetosis, liver failure, and classic Kayser-Fleischer rings at ophthalmologic examination. At MR imaging, cerebral atrophy and signal abnormalities are usually seen in the basal ganglia, cerebral white matter, midbrain, pons, and cerebellum.

Signal hyperintensity at T1-weighted imaging in patients with Wilson disease is most commonly found in the bilateral basal ganglia and ventrolateral thalami (Fig 17). The precise distribution of the signal abnormality correlates with clinical symptoms. Involvement of the striatum at MR imaging manifests with pseudoparkinsonian signs, dentatothalamic tract involvement manifests with cerebellar signs, pontocerebellar tract

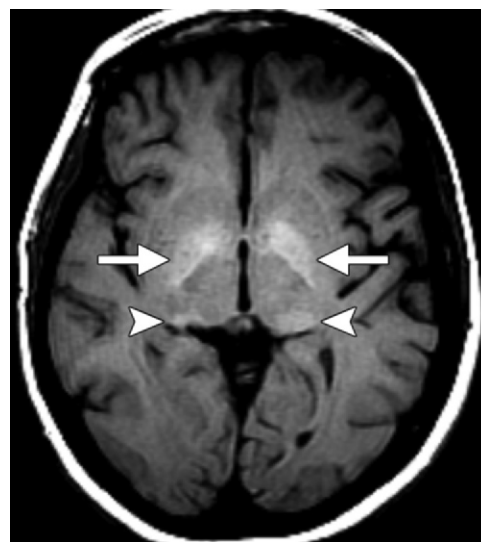


Figure 17. Wilson disease in a 49-year-old woman. Axial T1-weighted image shows bilateral regions of increased signal intensity within the globus pallidus (arrows) and thalamus (arrowheads).

involvement correlates with pseudoparkinsonian signs, and globus pallidus involvement is associated with portosystemic shunting secondary to cirrhosis (52). Regression of the signal abnormality at T1-weighted MR imaging correlates with response to treatment (53). T2-weighted sequences are also helpful, particularly with findings of signal hyperintensity in the midbrain combined with sparing of the superior colliculus, red nucleus, and portions of the substantia

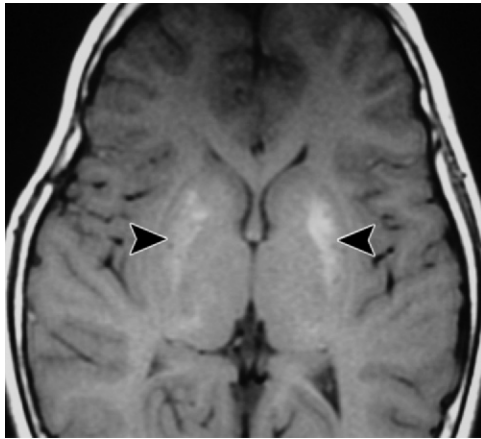


Figure 18. Type 1 neurofibromatosis in a 20-year-old man. Axial T1-weighted MR image shows bilateral symmetric regions of signal hyperintensity in the globus pallidus (arrowheads).

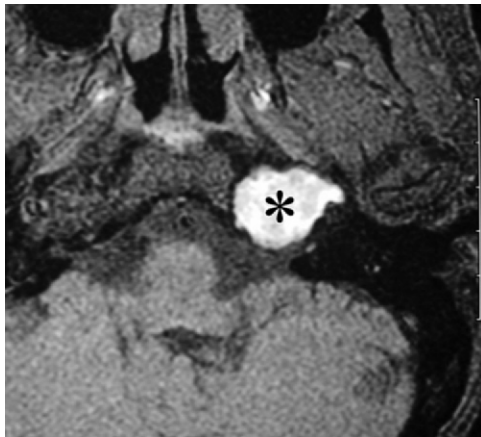


Figure 19. Cholesterol granuloma in a 40-year-old man. Axial T1-weighted fat-saturated MR image shows a large, well-defined, homogeneously hyperintense mass (*) at the left petrous apex that extends into the intracranial space posteriorly via a dehiscence in the posteromedial petrous apex cortical bone.

nigra; this combination of findings produces the “face of the giant panda” appearance on axial T2-weighted MR images (54).

Other Lesions

Type 1 Neurofibromatosis

Type 1 neurofibromatosis is an autosomal dominant disorder of the neurofibromin gene on chromosome 17 (55). With a worldwide incidence of approximately one case in 2500 to 3000 in the general population, type 1 neurofibromatosis is the

most common neurocutaneous syndrome (55). This syndrome has a wide variety of intracranial manifestations, including hypothalamic–optic nerve and brainstem pilocytic astrocytomas; neurofibromas; neurofibrosarcomas; plexiform neurofibromas; hydrocephalus; arachnoid cysts; cerebrovascular occlusions; nontumorous high-signal-intensity foci or unidentified bright objects that occur predominantly in the basal ganglia and posterior fossa on T2-weighted images; and high-signal-intensity lesions, distinct from unidentified bright objects, that most commonly appear in the basal ganglia on T1-weighted images (56–58). These T1-hyperintense basal ganglia lesions occur in approximately 20% of patients with type 1 neurofibromatosis (57,58) and predominantly involve the globus pallidus and internal capsules bilaterally and symmetrically (Fig 18). Extension of the high-signal-intensity region across the anterior commissure produces a dumbbell-like appearance (58). The etiology of these lesions is unclear, but they may be related to Schwann cell heterotopia, melanin, remyelination, microcalcifications, or a combination of these (57–59). The basal ganglia lesions in type 1 neurofibromatosis do not exhibit mass effect, surrounding edema, or enhancement.

Cholesterol Granuloma

Cholesterol granulomas are benign masses composed of proteinaceous debris and cholesterol crystals from blood breakdown secondary to obstruction and consequent chronic inflammatory foreign-body reaction (60,61). These lesions most commonly occur within the petrous apex but occasionally arise in the mastoid segment, middle ear, and orbitofrontal region (61,62). If sufficiently enlarged, cholesterol granulomas can cause bone dehiscence with resultant intracranial extension (61). Patients most commonly present with headache and hearing loss (63). Typically, cholesterol granulomas appear as smooth, well-defined, homogeneous masses that display high signal intensity at T1-weighted imaging (Fig 19). The high T1 signal of these lesions is unaffected by fat suppression techniques (62). Cholesterol granulomas are also often hyperintense at T2-weighted imaging and may display a hypointense rim secondary to hemosiderin deposition (61). Treatment of symptomatic lesions consists of surgical excision, drainage, or stenting (60). After successful drainage, cholesterol granulomas lose their T1 signal hyperintensity, whereas recurrent lesions tend to remain hyperintense (64).

Craniopharyngioma

Craniopharyngiomas are benign neoplasms derived from epithelial rests in the Rathke pouch (65). The main histopathologic subtypes are papillary, adamantinomatous, and mixed craniopharyngiomas. Papillary craniopharyngiomas tend to be solid and occur in adults, whereas the adamantinomatous variety tends to be cystic and occurs in children. Although most craniopharyngiomas are located in the suprasellar region, about half demonstrate an intrasellar component as well (66). An estimated 90% of craniopharyngiomas contain calcifications that are visible at CT and cystic components that sometimes show signal hyperintensity on T1-weighted images (Fig 20) (67). The T1 hyperintensity observed in the cystic components of craniopharyngiomas is attributable to the presence of protein, cholesterol granules, and methemoglobin (35). The cystic portions of craniopharyngiomas also frequently display T2 hyperintensity and rimlike enhancement on contrast-enhanced T1-weighted images (68).

Cortical Laminar Necrosis

Cortical laminar necrosis is a sequela of a global hypoxic ischemic event or, less commonly, an effect of immunosuppressive therapy or chemotherapy (69). The third layer of the cortex is particularly susceptible to depletion of oxygen and glucose (70). At MR imaging, a characteristic series of changes are seen in sequence: High-signal-intensity cortical lesions appear on T1-weighted images about 2 weeks after the inciting event and become increasingly conspicuous at 1–2 months after the event, along with maximum contrast enhancement (Fig 21) (71). T1 signal hyperintensity usually fades after 2 years, whereas parenchymal atrophy progresses. The high-signal-intensity features seen on T1-weighted images may be related to mineralization, protein denaturation, or lipid (72). However, methemoglobin does not appear to contribute to this signal hyperintensity (73).

Conclusions

Diverse categories of intracranial lesions appear bright at T1-weighted MR imaging. Familiarity with the types of substances and physical properties that contribute to T1 shortening is helpful for formulating an appropriate differential diagnosis and a systematic approach to the interpretation of high-signal-intensity lesions seen on T1-weighted images. Many disease entities have characteristic clinical and imaging features that allow definitive diagnosis.



Figure 20. Craniopharyngioma in a 2-year-old boy. Sagittal T1-weighted MR image shows a large mass (*) that contains multiple high-signal-intensity components (arrows).

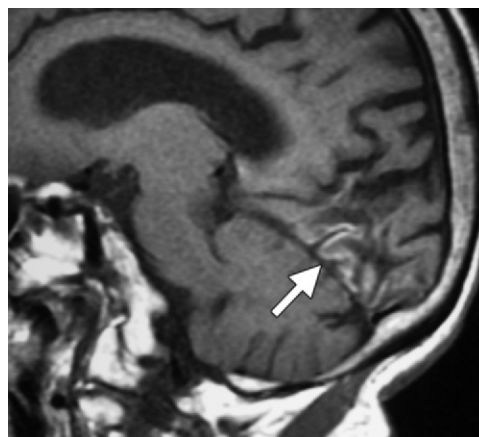


Figure 21. Cortical laminar necrosis in a 64-year-old man. Sagittal T1-weighted MR image demonstrates a gyriform region of high signal intensity in the occipital lobe cortex (arrow). The underlying brain parenchyma is atrophic.

References

- Jacobs MA, Ibrahim TS, Ouwkerk R. MR imaging: brief overview and emerging applications. *RadioGraphics* 2007;27(4):1213–1229.
- Bitar R, Leung G, Perng R, et al. MR pulse sequences: what every radiologist wants to know but is afraid to ask. *RadioGraphics* 2006;26(2):513–537.
- Takahashi M, Uematsu H, Hatabu H. MR imaging at high magnetic fields. *Eur J Radiol* 2003;46(1):45–52.
- Maubon AJ, Ferru JM, Berger V, et al. Effect of field strength on MR images: comparison of the same subject at 0.5, 1.0, and 1.5 T. *RadioGraphics* 1999;19(4):1057–1067.
- Bradley WG Jr. MR appearance of hemorrhage in the brain. *Radiology* 1993;189(1):15–26.
- Chao CP, Kotsenas AL, Broderick DF. Cerebral amyloid angiopathy: CT and MR imaging findings. *RadioGraphics* 2006;26(5):1517–1531.
- Knudsen KA, Rosand J, Karluk D, Greenberg SM. Clinical diagnosis of cerebral amyloid angiopathy: validation of the Boston criteria. *Neurology* 2001;56(4):537–539.

8. Zabramski JM, Wascher TM, Spetzler RF, et al. The natural history of familial cavernous malformations: results of an ongoing study. *J Neurosurg* 1994;80(3):422–432.
9. Yun TJ, Na DG, Kwon BJ, et al. A T1 hyperintense perilesional signal aids in the differentiation of a cavernous angioma from other hemorrhagic masses. *AJNR Am J Neuroradiol* 2008;29(3):494–500.
10. Petersen TA, Morrison LA, Schrader RM, Hart BL. Familial versus sporadic cavernous malformations: differences in developmental venous anomaly association and lesion phenotype. *AJNR Am J Neuroradiol* 2010;31(2):377–382.
11. Isensee C, Reul J, Thron A. Magnetic resonance imaging of thrombosed dural sinuses. *Stroke* 1994;25(1):29–34.
12. Poon CS, Chang JK, Swarnkar A, Johnson MH, Wasenko J. Radiologic diagnosis of cerebral venous thrombosis: pictorial review. *AJR Am J Roentgenol* 2007;189(6 Suppl):S64–S75.
13. Isiklar I, Leeds NE, Fuller GN, Kumar AJ. Intracranial metastatic melanoma: correlation between MR imaging characteristics and melanin content. *AJR Am J Roentgenol* 1995;165(6):1503–1512.
14. Enochs WS, Petherick P, Bogdanova A, Mohr U, Weissleder R. Paramagnetic metal scavenging by melanin: MR imaging. *Radiology* 1997;204(2):417–423.
15. Leach JL, Fortuna RB, Jones BV, Gaskill-Shipley MF. Imaging of cerebral venous thrombosis: current techniques, spectrum of findings, and diagnostic pitfalls. *RadioGraphics* 2006;26(Spec Issue):S19–S41; discussion S42–S43.
16. Escott EJ. A variety of appearances of malignant melanoma in the head: a review. *RadioGraphics* 2001;21(3):625–639.
17. Liubinas SV, Maartens N, Drummond KJ. Primary melanocytic neoplasms of the central nervous system. *J Clin Neurosci* 2010;17(10):1227–1232.
18. Smith AB, Rushing EJ, Smirniotopoulos JG. Pigmented lesions of the central nervous system: radiologic-pathologic correlation. *RadioGraphics* 2009;29(5):1503–1524.
19. Pirini MG, Mascacchi M, Salvi F, et al. Primary diffuse meningeal melanomatosis: radiologic-pathologic correlation. *AJNR Am J Neuroradiol* 2003;24(1):115–118.
20. Henkelman RM, Watts JF, Kucharczyk W. High signal intensity in MR images of calcified brain tissue. *Radiology* 1991;179(1):199–206.
21. Warakaulle DR, Anslow P. Differential diagnosis of intracranial lesions with high signal on T1 or low signal on T2-weighted MRI. *Clin Radiol* 2003;58(12):922–933.
22. Hood MN, Ho VB, Smirniotopoulos JG, Szumowski J. Chemical shift: the artifact and clinical tool revisited. *RadioGraphics* 1999;19(2):357–371.
23. Truwit CL, Barkovich AJ. Pathogenesis of intracranial lipoma: an MR study in 42 patients. *AJR Am J Roentgenol* 1990;155(4):855–864; discussion 865.
24. Jabot G, Stoquart-Elsankari S, Saliou G, Toussaint P, Deramond H, Lehmann P. Intracranial lipomas: clinical appearances on neuroimaging and clinical significance. *J Neurol* 2009;256(6):851–855.
25. Yildiz H, Hakyemez B, Koroglu M, Yesildag A, Baykal B. Intracranial lipomas: importance of localization. *Neuroradiology* 2006;48(1):1–7.
26. Smirniotopoulos JG, Chiechi MV. Teratomas, dermoids, and epidermoids of the head and neck. *RadioGraphics* 1995;15(6):1437–1455.
27. Isaacs H Jr. I. Perinatal brain tumors: a review of 250 cases. *Pediatr Neurol* 2002;27(4):249–261.
28. Liu JK, Gottfried ON, Salzman KL, Schmidt RH, Couldwell WT. Ruptured intracranial dermoid cysts: clinical, radiographic, and surgical features. *Neurosurgery* 2008;62(2):377–384; discussion 384.
29. Osborn AG, Preece MT. Intracranial cysts: radiologic-pathologic correlation and imaging approach. *Radiology* 2006;239(3):650–664.
30. Stendel R, Pietilä TA, Lehmann K, Kurth R, Suess O, Brock M. Ruptured intracranial dermoid cysts. *Surg Neurol* 2002;57(6):391–398; discussion 398.
31. Ruchoux MM, Kepes JJ, Dhellemmes P, et al. Lipomatous differentiation in ependymomas: a report of three cases and comparison with similar changes reported in other central nervous system neoplasms of neuroectodermal origin. *Am J Surg Pathol* 1998;22(3):338–346.
32. Chang WE, Finn LS. MR appearance of lipomatous ependymoma in a 5-year-old boy. *AJR Am J Roentgenol* 2001;177(6):1475–1478.
33. Fullerton GD, Finnie MF, Hunter KE, Ord VA, Cameron IL. The influence of macromolecular polymerization of spin-lattice relaxation of aqueous solutions. *Magn Reson Imaging* 1987;5(5):353–370.
34. Som PM, Dillon WP, Fullerton GD, Zimmerman RA, Rajagopalan B, Marom Z. Chronically obstructed sinonasal secretions: observations on T1 and T2 shortening. *Radiology* 1989;172(2):515–520.
35. Armao D, Castillo M, Chen H, Kwock L. Colloid cyst of the third ventricle: imaging-pathologic correlation. *AJNR Am J Neuroradiol* 2000;21(8):1470–1477.
36. Sumida M, Uozumi T, Mukada K, Arita K, Kurisu K, Eguchi K. Rathke cleft cysts: correlation of enhanced MR and surgical findings. *AJNR Am J Neuroradiol* 1994;15(3):525–532.
37. Binning MJ, Gottfried ON, Osborn AG, Couldwell WT. Rathke cleft cyst intracystic nodule: a characteristic magnetic resonance imaging finding. *J Neurosurg* 2005;103(5):837–840.
38. Kim JE, Kim JH, Kim OL, et al. Surgical treatment of symptomatic Rathke cleft cysts: clinical features and results with special attention to recurrence. *J Neurosurg* 2004;100(1):33–40.
39. Mitchell LA, Thomas PQ, Zacharin MR, Scheffer IE. Ectopic posterior pituitary lobe and periventricular heterotopia: cerebral malformations with the same underlying mechanism? *AJNR Am J Neuroradiol* 2002;23(9):1475–1481.
40. van der Linden AS, van Es HW. Case 112: pituitary stalk transection syndrome with ectopic posterior pituitary gland. *Radiology* 2007;243(2):594–597.
41. Fujisawa I, Kikuchi K, Nishimura K, et al. Transection of the pituitary stalk: development of an ectopic posterior lobe assessed with MR imaging. *Radiology* 1987;165(2):487–489.
42. Castillo M. Pituitary gland: development, normal appearances, and magnetic resonance imaging protocols. *Top Magn Reson Imaging* 2005;16(4):259–268.

43. Kurokawa H, Fujisawa I, Nakano Y, et al. Posterior lobe of the pituitary gland: correlation between signal intensity on T1-weighted MR images and vasopressin concentration. *Radiology* 1998;207(1):79–83.
44. Koob M, Laugel V, Durand M, et al. Neuroimaging in Cockayne syndrome. *AJNR Am J Neuroradiol* 2010;31(9):1623–1630.
45. McNeill A, Chinnery PF. Neurodegeneration with brain iron accumulation. *Handb Clin Neurol* 2011;100:161–172.
46. Sener RN. Pantothenate kinase-associated neurodegeneration: MR imaging, proton MR spectroscopy, and diffusion MR imaging findings. *AJNR Am J Neuroradiol* 2003;24(8):1690–1693.
47. Hayflick SJ, Hartman M, Coryell J, Gitschier J, Rowley H. Brain MRI in neurodegeneration with brain iron accumulation with and without PANK2 mutations. *AJNR Am J Neuroradiol* 2006;27(6):1230–1233.
48. Rovira A, Alonso J, Córdoba J. MR imaging findings in hepatic encephalopathy. *AJNR Am J Neuroradiol* 2008;29(9):1612–1621.
49. Pujol A, Pujol J, Graus F, et al. Hyperintense globus pallidus on T1-weighted MRI in cirrhotic patients is associated with severity of liver failure. *Neurology* 1993;43(1):65–69.
50. Pujol J, Kulisevsky J, Moreno A, et al. Neurospectroscopic alterations and globus pallidus hyperintensity as related magnetic resonance markers of reversible hepatic encephalopathy. *Neurology* 1996;47(6):1526–1530.
51. Lorincz MT. Neurologic Wilson's disease. *Ann NY Acad Sci* 2010;1184:173–187.
52. van Wassenaeer-van Hall HN, van den Heuvel AG, Algra A, Hoogenraad TU, Mali WP. Wilson disease: findings at MR imaging and CT of the brain with clinical correlation. *Radiology* 1996;198(2):531–536.
53. Kim TJ, Kim IO, Kim WS, et al. MR imaging of the brain in Wilson disease of childhood: findings before and after treatment with clinical correlation. *AJNR Am J Neuroradiol* 2006;27(6):1373–1378.
54. Thapa R, Ghosh A. 'Face of the giant panda' sign in Wilson disease. *Pediatr Radiol* 2008;38(12):1355.
55. Williams VC, Lucas J, Babcock MA, Gutmann DH, Korf B, Maria BL. Neurofibromatosis type 1 revisited. *Pediatrics* 2009;123(1):124–133.
56. Jacques C, Dietemann JL. Imaging features of neurofibromatosis type 1 [in French]. *J Neuroradiol* 2005;32(3):180–197.
57. Terada H, Barkovich AJ, Edwards MS, Ciricillo SM. Evolution of high-intensity basal ganglia lesions on T1-weighted MR in neurofibromatosis type 1. *AJNR Am J Neuroradiol* 1996;17(4):755–760.
58. Mirowitz SA, Sartor K, Gado M. High-intensity basal ganglia lesions on T1-weighted MR images in neurofibromatosis. *AJR Am J Roentgenol* 1990;154(2):369–373.
59. DiPaolo DP, Zimmerman RA, Rorke LB, Zackai EH, Bilaniuk LT, Yachnis AT. Neurofibromatosis type 1: pathologic substrate of high-signal-intensity foci in the brain. *Radiology* 1995;195(3):721–724.
60. Royer MC, Pensak ML. Cholesterol granulomas. *Curr Opin Otolaryngol Head Neck Surg* 2007;15(5):319–322.
61. Chapman PR, Shah R, Curé JK, Bag AK. Petrous apex lesions: pictorial review. *AJR Am J Roentgenol* 2011;196(3 suppl):WS26–WS37.
62. Chow LP, McNab AA. Orbitofrontal cholesterol granuloma. *J Clin Neurosci* 2005;12(2):206–209.
63. Thedinger BA, Nadol JB Jr, Montgomery WW, Thedinger BS, Greenberg JJ. Radiographic diagnosis, surgical treatment, and long-term follow-up of cholesterol granulomas of the petrous apex. *Laryngoscope* 1989;99(9):896–907.
64. Greenberg JJ, Oot RF, Wismer GL, et al. Cholesterol granuloma of the petrous apex: MR and CT evaluation. *AJNR Am J Neuroradiol* 1988;9(6):1205–1214.
65. Prabhu VC, Brown HG. The pathogenesis of craniopharyngiomas. *Childs Nerv Syst* 2005;21(8-9):622–627.
66. Zada G, Lin N, Ojerholm E, Ramkissoon S, Laws ER. Craniopharyngioma and other cystic epithelial lesions of the sellar region: a review of clinical, imaging, and histopathological relationships. *Neurosurg Focus* 2010;28(4):E4.
67. Curran JG, O'Connor E. Imaging of craniopharyngioma. *Childs Nerv Syst* 2005;21(8-9):635–639.
68. Ahmadi J, Destian S, Apuzzo ML, Segall HD, Zee CS. Cystic fluid in craniopharyngiomas: MR imaging and quantitative analysis. *Radiology* 1992;182(3):783–785.
69. Bargalló N, Burrell M, Berenguer J, Cofan F, Buñesch L, Mercader JM. Cortical laminar necrosis caused by immunosuppressive therapy and chemotherapy. *AJNR Am J Neuroradiol* 2000;21(3):479–484.
70. Kuroiwa T, Okeda R. Neuropathology of cerebral ischemia and hypoxia: recent advances in experimental studies on its pathogenesis. *Pathol Int* 1994;44(3):171–181.
71. Siskas N, Lefkopoulos A, Ioannidis I, Charitandi A, Dimitriadis AS. Cortical laminar necrosis in brain infarcts: serial MRI. *Neuroradiology* 2003;45(5):283–288.
72. Shan DE. Delayed ischemic hyperintensity of T1-weighted MRI. *Stroke* 2000;31(3):797–798.
73. Niwa T, Aida N, Shishikura A, Fujita K, Inoue T. Susceptibility-weighted imaging findings of cortical laminar necrosis in pediatric patients. *AJNR Am J Neuroradiol* 2008;29(9):1795–1798.

Intracranial Lesions with High Signal Intensity on T1-weighted MR Images: Differential Diagnosis

Daniel T. Ginat, MD, MS • Steven P. Meyers, MD, PhD

RadioGraphics 2012; 32:499–516 • Published online 10.1148/rg.322105761 • Content Codes:  

Page 500

Only a few naturally occurring substances are known to reduce T1 relaxation times, and the extent of that reduction depends on their occurrence in substantial concentrations. These substances include methemoglobin, melanin, lipid, protein, and minerals.

Page 502 (Figure on page 502)

Subacute hemorrhage and degraded blood products within the lesion produce a halo of signal hyperintensity around the lesion on T1-weighted images, a useful finding for differentiating cavernous malformations from hemorrhagic tumors and other intracranial hemorrhages (9) (Fig 2b).

Page 507 (Figure on page 507)

Dermoid cyst rupture is a rare complication that can cause severe chemical meningitis and sensory or motor hemisyndrome (28,30). This complication manifests at T1-weighted MR imaging as scattered high-signal-intensity foci within the ventricles or subarachnoid spaces (Fig 9).

Page 511 (Figure on page 512)

At MR imaging, hepatic encephalopathy characteristically manifests as bilateral regions of signal hyperintensity in the lentiform nucleus and substantia nigra on T1-weighted images (Fig 16). These regions of abnormally high signal intensity at T1-weighted imaging are related to the accumulation of manganese in patients with hepatic encephalopathy and may be encountered also in welders and recipients of hyperalimentation therapy.

Page 512 (Figure on page 512)

Signal hyperintensity at T1-weighted imaging in patients with Wilson disease is most commonly found in the bilateral basal ganglia and ventrolateral thalami (Fig 17). The precise distribution of the signal abnormality correlates with clinical symptoms.